Microbe-metabolite associations linked to the rebounding murine gut microbiome post-colonization with vancomycin resistant *Enterococcus faecium*

Andre Mu[a,b,c], Glen P. Carter[a], Lucy Li[a], Nicole S. Isles[a,c], Alison F. Vrbanac[d,e], James T. Morton[f], David P. De Souza[g], Vinod K. Narayana[g], Komal Kanojia[h], Brunda Nijagal[g], Malcolm J. McConville[g,i], Rob Knight[d,e,j,k], Benjamin P. Howden[a,b,c] and Timothy P. Stinear[a,b]#

[a]Department of Microbiology and Immunology at the Peter Doherty Institute for Infection and Immunity, University of Melbourne, Australia

[b]Doherty Applied Microbial Genomics, Department of Microbiology and Immunology at the Peter Doherty Institute for Infection and Immunity, Australia

[c]Microbiological Diagnostic Unit Public Health Laboratory, at the Peter Doherty Institute for Infection and Immunity, University of Melbourne, Australia

[d]Department of Pediatrics, University of California San Diego, USA

[e]Department of Computer Science & Engineering, University of California San Diego, USA

[f]Flatiron Institute, Centre for Computational Biology, USA

[g]Metabolomics Australia, Bio21 Institute of Molecular Science and Biotechnology, University of Melbourne, Australia

[h]Centre for Biostatistics and Clinical Trials, Peter MacCallum Cancer Centre, Victoria, Australia

[i]Department of Biochemistry and Molecular Biology, University of Melbourne, Australia

[j]Department of Bioengineering, University of California San Diego, USA

[k]Center for Microbiome Innovation, University of California San Diego, USA

Running head: Gut microbiome and colonization with VRE

#Address correspondence to Professor Timothy P. Stinear**,** tstinear@unimelb.edu.au

B.P.H and T.P.S contributed equally to this work.

Word count: 2,473

mSystems Host-Microbe Biology

Keywords

Microbiome, multi-omics, metagenomics, metabolomics, gut microbiome, vancomycin resistant *Enterococci*, colonization, antimicrobial resistance

Abstract

Vancomycin resistant *Enterococcus faecium* (VREfm) is an emerging antibiotic resistant pathogen. Strain-level investigations are beginning to reveal the molecular mechanisms used by VREfm to colonize regions of the human bowel. However, the role of commensal bacteria during VREfm colonization, in particular following antibiotic treatment, remains largely unknown. We employed amplicon 16S rRNA gene sequencing and metabolomics in a murine model system to try and investigate functional roles of the gut microbiome during VREfm colonization. First-order taxonomic shifts in gut microbial community composition were detected both in response to pretreatment using ceftriaxone, and to subsequent VREfm challenge. Using neural networking approaches to find co-occurrence profiles of bacteria and metabolites, we detected key metabolome features during and after VREfm colonization. These metabolite features were associated with *Bacteroides*, indicative of a transition towards a pre-antibiotic naïve microbiome. This study shows the impacts of antibiotics on the gut ecosystem, and the progression of the microbiome in response to colonisation with VREfm. Our results

offer insights towards identifying potential non-antibiotic alternatives to eliminate VREfm through metabolic re-engineering to preferentially select for *Bacteroides*.

Importance

This study demonstrates the importance and power of linking bacterial composition profiling with metabolomics to find the interactions between commensal gut bacteria and a specific pathogen. Knowledge from this research will inform gut microbiome engineering strategies, with the aim of translating observations from animal models to human-relevant therapeutic applications.

Introduction

Vancomycin-resistant *Enterococcus faecium* (VREfm) is a significant healthcare-associated pathogen. VREfm infections can be difficult to treat due to their intrinsic and acquired resistance to nearly all classes of antibiotics (1). The World Health Organisation categorizes VREfm as a "High Priority" bacterial pathogen, advocating research to stop the global increase in antibiotic resistance (2). Recent studies highlight the importance of the gut microbiota in modulating the growth and virulence of VRE*fm* in the gastrointestinal ecosystem. For instance, the depletion of normal gut flora using antibiotics exacerbates the severity of VREfm infection (3), whereas transplant of commensal species including a consortium of *Clostridium bolteae*, *Blautia producta*, *Blautia sartorii*, and *Parabacteroides distasonis* (4, 5) can drive established VREfm colonisation to below levels of culture detection. Specifically, *B. producta* – a colonizer of the colon – reduces VREfm growth *in vivo* by secreting a lantibiotic (6). These observations raise the intriguing possibility that metabolic traits act in concert between pathogen and select gut commensals to confer mutual benefits during pathogen persistence.

76 These findings also highlight the greater risk posed to immunocompromised patients when
77 colonized with VREfm. For instance, allogeneic hematopoietic cell transplantation patients
78 have gastrointestinal tracts that are dominated by VREfm as a result of losing a large portion
79 of the intestinal commensal microbiota upon receiving broad-spectrum antibiotics as pre-
80 treatment(7). Hildebrand et al., (2018) discovered long-term ecological impacts to the gut
81 microbiome, with strong bacterial species turnover, after ceftriaxone treatment in humans (8).
82 Further, mice receiving broad spectrum antibiotics (combination of metronidazole, neomycin,
83 and vancomycin) showed markedly increased VREfm colonization of the caecum and colon.
84 The compromised intestinal innate immune defenses in these animals allowed proliferation of
85 VREfm caused by the antibiotic exposure and subsequently reduced the expression of
86 antimicrobial molecules produced by bacteria in the intestinal mucosa(9).

87 The problem with VREfm is further complicated by the fact that *Enterococci* are
88 members of the gastrointestinal tract microbiota; a key reservoir of antimicrobial resistance
89 (AMR) genes, and potentially facilitating gene transfer within the gut microbiome(10). For
90 example, the *vanB* resistance gene was detected in human faecal specimens that did not contain
91 culturable VRE; and instead, demonstrated that isolates carrying the resistance transposon are
92 anaerobic commensal bacteria, *Eggerthella lenta* and *Clostridium innocuum*(11). Colonisation
93 of, and persistence in, the gastrointestinal tract therefore presents as a key mechanism for *de*
94 *novo* VRE and may lead to severe invasive disease.

95

96 This current study aimed to understand the impact of antibiotics on the murine gut microbiota,
97 and the subsequent colonisation pattern of VREfm. To this extent, we designed a murine model
98 time-series study that consisted of two main perturbative phases: (1) antibiotic pre-treatment
99 with ceftriaxone, and (2) VREfm challenge. Our 16S rRNA profiling analyses highlighted a
100 first-order shift in bacterial biodiversity composition across time, a second-order clustering of

101 samples associated with the experimental phases, and the transition of the post-VREfm
102 colonisation gut microbiota and its metabolome towards resembling an asymptomatic carriage-
103 like microbiome phenotype. This research provides support for engineering the metabolic
104 potential of the gut microbiome using, for example, prebiotics as a non-antibiotic alternative
105 for treating multi-drug resistant bacterial infections.
106
107 **Results**
108 *Experimental design*
109 The following experimental design was developed to address the hypothesis that there are
110 specific murine gut microbiome factors that facilitates VREfm colonization; three groups of
111 three C57BL/6 mice (co-caged wildtype males) were monitored, and fecal samples collected,
112 over a fourteen-day period with two intervention time-points; including (1) a two-day
113 ceftriaxone treatment administered at 0.5g/L in drinking water, and (2) colonisation (via oral-
114 gavage) with 1 x 10^6 VREfm ST796 per mice post-antibiotic treatment. Mice were housed in
115 groups of three to represent three technical replicates per cage; herein, each group of three co-
116 housed mice will be referred to as Group A, Group B, and Group C. Table 1 highlights samples
117 and datasets collected.
118
119 *Amplicon 16S rRNA gene sequencing revealed first order shifts in bacterial community*
120 *composition.*
121 Amplicon 16S rRNA gene sequencing was performed to capture the bacterial community
122 composition in an effort to track changes in response to antibiotic pre-treatment and VREfm
123 colonization. Bacterial community profiles were assessed in fecal samples from nine mice
124 before, during and after the two interventions (Table 1). A total of 71.32% of reads (10,519,073
125 reads) passed quality control, with 321,955 reads on average per sample and a total of 3574

126 exact variant sequence types (i.e., features), with an average of 118 features per sample, and
127 an upper bound of 246 features (when rarefied to 20,000 reads). Alpha rarefaction analysis
128 demonstrated sufficient sequencing depth to capture microbial diversity to saturation
129 (Supplementary Figure 1).

130 The biodiversity profiles of each sample were compared and showed that key sOTUs
131 were differentially abundant throughout the course of the experiment. Of note, there was a shift
132 in the dominance of Bacteroidia (Bacteroidetes; light green coloured bars) during the naïve
133 phase of the experiment to Mollicutes (Tenericutes; pink coloured bars) in response to
134 ceftriaxone treatment, with a return to the predominance of Bacteroidia during the late-phase
135 of the experiment, post-VREfm colonisation (i.e., days 12 – 14).

136

137 *The murine gut microbiota responds to antibiotics and microbial community richness begins*
138 *to rebound three-days post-VRE colonisation*

139 Principal coordinate analysis (PCoA) of the unweighted UniFrac(12) distances was used to
140 assess clustering of fecal samples based on bacterial composition. This assessment showed that
141 the fecal microbiota from samples collected from each phase clustered together but were
142 clearly separated between phases; after exposure to ceftriaxone, and challenge with VREfm
143 post-antibiotic treatment (Figure 2A). Permutation-based statistical testing demonstrates the
144 groups are significantly different from one another (Supplementary Figure 2). Temporal
145 tracking of the changing microbiomes against each mouse on the PCoA sample-space
146 demonstrated a clear, unidirectional trajectory that followed the chronology of the experiment
147 (animation as a supplementary file). Procrustes analyses of weighted and unweighted UniFrac
148 distances showed that the same general patterns on the sample space were preserved, meaning
149 that there is congruency in global spatial patterns between qualitative and quantitative measures
150 of community dissimilarity (Supplementary Figure 3).

151 Analysis of community diversity (Faith's Phylogenetic Diversity Index) revealed a
152 stable and rich microbial community during the naïve phase preceding a sharp decrease
153 following antibiotic treatment, and a further decrease immediately following VREfm
154 colonisation (Figure 2B). Of note is the responsiveness of the microbiota (within 24 hours) to
155 the removal of antibiotics at the end of day 7. Community richness began to rebound at
156 approximately three-days post-VREfm colonisation (i.e., day 12), with Group A demonstrating
157 a faster rate of rebound compared to Group B and C. Calculating the distances of dissimilarity
158 (unweighted UniFrac distances) of each mouse microbiota timepoint relative to Day 0 (a proxy
159 for the naive bacterial community phenotype) revealed a small dissimilarity distance for
160 samples collected during the naïve phase, and an increasing dissimilarity distance following
161 antibiotic treatment (day 6) and VREfm colonisation (day 9; Figure 2C). There was a
162 downward trajectory in distance scores at three-days post-VREfm colonisation (i.e., day 12);
163 Group A followed a sharper return to a microbiota resembling day 0. These observations
164 suggest that mice were transitioning towards a persistent carrier-like state, and that the
165 rebounding community richness towards levels representative of the naïve phase was by a
166 microbial community structure that resembled the naïve phase. Additional studies, where the
167 time-frame post-VREfm challenge extends beyond one-week of monitoring, are needed.
168
169 *Multinomial regression identifies sOTUs most positively associated with VREfm colonisation*
170 Multinomial regression using *Songbird* was employed to identify sOTUs that were most
171 positively, and negatively, associated with the post-VREfm colonisation phase (Figure 3). The
172 five most positively associated sOTUs were *Enterococcus*, *Bacteroides*, *Erysipelotrichaceae*,
173 *Catabacter*, and *Lachnospiraceae*; while the five most negatively associated were
174 *Clostridiales*, *Adlercreutzia*, *Mollicutes*, *Peptostreptococcaceae*, and *Clostridiales*. Temporal
175 tracking of exact sequence variants (ESV) demonstrated that the ESV feature classified as

176 *Enterococcus* - and identified as the most positively associated with the post-VREfm
177 colonisation phase - was most abundant on days of challenge; confirming that this ESV likely
178 was the ST796 VREfm colonization challenge organisms. There were a further eight ESV
179 features classified as *Enterococcus*, however, they were absent during the days representing
180 VREfm colonisation, and lacked positive associations with the post-VREfm colonisation
181 phase, suggesting that these features represent murine gut commensal Enterococci.
182
183 *Molecular networking identifies differential metabolome profiles*
184 Duplicate fecal samples from key timepoints throughout the experiment (i.e., days 0, 5, 6, 7, 8,
185 9, and 14) were analysed by data dependent tandem mass spectrometry (MSMS) performed on
186 a liquid-chromatography quadrupole time-of-flight (LC-QTOF) to monitor changes in the
187 murine gut metabolome (Table 1). Mass spectrometry in both positive and negative polarity
188 identified 627 spectra with library hits through the Global Natural Products Social Molecular
189 Networking (GNPS;(13)). Analysis of the global metabolome profile of each sample was
190 measured based on their overlapping molecules, and a PCoA plot using a binary Jaccard
191 distance metric; a qualitative measure of sample dissimilarity. A separation of metabolite
192 profiles along PCoA1 was observed (57.34% Figure 4A). Metabolomes from the naïve, and
193 late-VREfm colonisation phase tended to cluster together, while samples from the post-
194 antibiotic phases including the early-VREfm colonisation phase clustered together
195 (Supplementary Figure 4 with supporting pairwise PERMANOVA testing).
196 Random forest analysis of spectra profiles from LC-MSMS was used to predict
197 experimental phase and rank the importance of metabolite association with each experimental
198 phase. The top metabolite features for each experimental phase are highlighted in Figure 4B.
199 Unique profiles of metabolite features were observed for each phase of the experiment.
200 Importantly, the late-VREfm colonisation phase captures an unknown metabolite with a mass-

201 to-charge ratio (m/z) of 173.067 and retention time (RT) of 18.392; this metabolite is
202 exclusively present during what represents the *transition* towards resembling the naïve
203 microbiome.
204
205 *Bacteroidales-associated metabolites implicated in late-phase post-VREfm colonisation*
206 A distinct profile shift in microbe and metabolite abundances (as calculated by multinomial
207 regression) was observed, particularly during late-phase VREfm colonisation (Supplementary
208 Figure 5). Shallow neural networking analysis with *mmvec* was used to predict microbe-
209 metabolite interactions through their co-occurrence probabilities (Figure 5). Sequential biplots
210 captured the shift in experimental phases and highlighted the co-occurrences of microbiota and
211 metabolomic datasets (Fig. 5A,B). There was a strong *Enterococcus* effect as indicated by the
212 magnitude of the corresponding arrow, and the rebounding species during the late-phase
213 VREfm colonisation are predominantly *Bacteroidales* sOTUs (Figure 5C); with the co-
214 occurring metabolite features m/z 173.067 RT 18.392, and m/z 167.083 RT 25.277. Metabolite
215 feature mz 245.055 RT 7.945 was ranked as being highly associated with the post-VRE
216 colonisation phase. These results integrate microbial and metabolite datasets to suggest which
217 microbes may be responsible for a particular metabolite. In this instance, the metabolite
218 exclusively present during what a *transition* towards the original naïve microbiome resembles
219 (m/z 173.067 and RT 18.392; Figure 5B) is linked with *Bacteroidales*.
220
221 **Discussion**
222 In this study of the murine gut ecosystem, we employed a mouse model of gastrointestinal tract
223 colonisation that replicates the shift in bacterial composition when patients enter the healthcare
224 system, develop an imbalance in microbiome as a result of pre-treatment (e.g., antibiotic
225 treatment), and are subsequently colonised with a hospital superbug (14). The resolution of

226 current studies describes a consortium of commensal microbes that can, for example, reduce
227 the magnitude of VREfm colonisation (4, 6); however, understanding the key metabolic shifts
228 relative to the gut microbiota remains challenging (15). Here, we employed amplicon 16S
229 rRNA gene sequencing and high-resolution mass spectrometry metabolomics in an effort
230 towards determining microbiota-metabolome interactions during VREfm colonisation. We
231 demonstrated clear changes in the gut microbiome in response to ceftriaxone and VREfm
232 challenge.
233
234 Conceptual and statistical advances in analysis of amplicon 16S rRNA gene data (16, 17)
235 whereby OTUs are clustered at a 99% nucleotide similarity threshold allows for the
236 identification of exact sequence variants (ESV). Query against an error-corrected database
237 (17)can detect multiple ESVs that may be classified to the same taxonomic rank. For example,
238 our analyses identified multiple ESVs classified as *Enterococci*; however, when the relative
239 abundances were tracked across the chronology of the experiment, only one *Enterococci*-ESV
240 was dominant in relative abundances and most positively associated with the days of post-
241 VREfm challenge. This highlights the resolving power to differentiate between commensal and
242 pathogenic strains of *Enterococci* when the composition of the microbial community is
243 considered. The fact that this was achievable at the level of amplicon 16S rRNA gene
244 sequencing alludes to the possibility of implementing microbiota screenings as routine
245 diagnostics for patients entering healthcare systems. Further, first-order level shifts in
246 microbial community composition was observed in response to ceftriaxone and subsequent
247 VREfm challenge (Figure 1). At three days post-VREfm colonisation (i.e., day 12), the
248 microbiome richness begins to rebound; suggesting that mice are transitioning towards a
249 persistent carrier-like state. Interestingly, Group A cohort exhibited a faster rate of rebound
250 that may be facilitated by their initially higher microbial community richness (Figure 2B); this

251 observation supports the need to prescreen "baseline" microbiota profiles of patients upon
252 admission into hospitals. We can begin to assess patients from across different wards (e.g.,
253 intensive care unit, oncology, neurology, and healthy cohorts), and build a database of
254 microbiome profiles that can be used as biomarkers to predict: (1) the susceptibility of patients
255 to develop persistent bacterial colonisation, and (2) propensity to clear the pathogen once
256 colonized. The clinical implication is that new patients are screened and identified (via beta-
257 diversity meta-analyses) by these biomarkers and placed in bedding cohorts accordingly;
258 thereby improving infectious disease management and isolation precautions within health-care
259 associated ecosystems.
260
261 The shortlist of microbes ranked as most negatively associated with the colonisation phase
262 (*Clostridiales*, *Adlercreutzia*, *Mollicutes*, *Peptostreptococcaceae*, and *Clostridiales*) are
263 hypothesized to play a role in maintaining the health of the animals. Indeed, amongst the
264 microbes identified, are known short chain fatty acid (e.g., butyric acid) producers (18, 19) that
265 supports, and expands upon those previously identified by Caballero et al., (2017). Further, the
266 use of Deblur to identify ESVs facilitates the temporal tracking of their relative abundances to
267 inform selection of primary fecal samples that will provide the best probability (i.e., highest
268 relative abundance) of culturing target taxa for downstream screening of probiotic potential.
269 However, translating animal-derived observations from experimental animal models to human
270 clinical situations remains challenging; particularly where the key microbes are rodent-
271 specific. One solution may be to integrate metabolomics to reveal shared metabolic capacity
272 amongst taxonomically divergent microbes. Our supervised classifying approaches suggests
273 an altered metabolome composition during the late-phase of VREfm challenge that may
274 facilitate the apparent "suppression" of VREfm to levels below the limit-of-detection by
275 culture. Despite the caveat of poor resolution in current databases to link metabolite features

276 to associated chemical structures, microbe-metabolite vector analysis linked one metabolite to
277 *Bacteroides* (m/z 173.067); permitting strain-level omics in an effort to comprehensively
278 annotate the metabolome. Further research to comprehensively characterize interactions
279 between microbe and metabolome will be critical to address the gaps in our understanding of
280 the biochemical parameters of the microbiome.
281
282 The resolution of our results provides the basis in which to begin to identify non-antibiotic
283 alternatives to engineer the gut microbiome and translating animal studies to human-relevant
284 therapeutic applications. Here, achieving integrative omics to link microbe-metabolite
285 associations, adds support to the incorporation of this approach to microbiome profiling into
286 routine clinical microbiology, particularly in the context of monitoring the impacts of antibiotic
287 use.
288
289 **Methods**
290 *Mouse gastrointestinal colonization model*
291 Wild type C57BL/6 male mice were used to establish an animal model of gastrointestinal
292 colonisation with VREfm. Mice were pretreated with 0.5 g/L ceftriaxone in drinking water for
293 two-days followed by an antibiotic wean period of 24hrs. Mice were then colonized with 1 x
294 10^6 cfu VREfm ST796.
295
296 *Genomic DNA extraction and sequencing*
297 Whole community gDNA was extracted from mouse faecal samples using the Qiagen
298 PowerSoil DNA Extraction Kit (formerly MoBio) following the manufacturer's protocol. A
299 preprocessing step of mechanical lysis was incorporated using a Bertin Technologies
300 Precellysis 24 machine for one round of a 40 second-cycle at 6000 rpm. The V4 region of the

301 bacterial 16S rRNA gene was amplified using small subunit 515 forward Golay-barcoded, and
302 SSU806 reverse primers following the Earth Microbiome Project protocol
303 (www.earthmicrobiome.org;(20)), and sequenced using the Illumina MiSeq platform (V2, 300
304 cycles; Illumina Inc., San Diego, USA). Sample metadata and sequence data for the current
305 study were deposited into *QIITA* (21) - an open-source management platform for research
306 studies with multiple 'omic datasets - under the project title *Mouse-hospital VRE colonization*
307 *with ceftriaxone treatment* (Study ID 11737). Raw sequence data are also available through the
308 NCBI SRA, BioProject number: PRJNA590613
309
310 *Amplicon 16S rRNA gene profiling analyses*
311 Sequence data were processed within the *QIITA* framework for quality control (split libraries),
312 demultiplexing, trimming sequence reads to a length of 150 nt, and picking sub-operational
313 taxonomic units (sOTUs) using *Deblur* to resolve single-nucleotide community sequencing
314 patterns (*i.e.* feature identification of sOTUs;(17)). The output BIOM files were further
315 processed using *QIIME2* for downstream statistical analyses(22). Alpha rarefaction curves
316 were generated to determine if each sample had been sequenced to saturation; the feature table
317 was subsequently rarefied to 20,000 reads per sample. Taxonomy was assigned using the
318 *sklearn* classifier (23) and *Greengenes 13.8 99% OTUs from 515F/806R region of sequences*
319 classifier available from https://docs.qiime2.org/2018.4/data-resources/. Furthermore, relative
320 abundances of each taxa were visualized as bar plots using the QIIME2 *taxa* plugin. A
321 phylogenetic tree was constructed using fragment-insertion (*QIIME fragment-insertion sepp;*
322 (24)) to guide phylogenetic-aware statistical analyses generated using the *QIIME2* plugin, *q2-*
323 *diversity core-metrics-phylogenetic*; key metrics computed by default include both alpha-
324 diversity (e.g., Shannon's diversity index, Faith's phylogenetic diversity, and Evenness), and
325 beta-diversity (e.g., Bray-Curtis distance, and unweighted UniFrac distances) metrics. The

326 unweighted UniFrac distance matrix (12) was used to compute first distances and calculate
327 distances relative to Day 0 as baseline between sequential states (*QIIME longitudinal first-*
328 *distances*); *ggplot2* (R, https://ggplot2.tidyverse.org) was used to visualize the distance scores
329 as line plots. *Emperor* was used to visualize principal coordinate analysis plots of unweighted
330 UniFrac distances. Permutation-based statistical testing (PERMANOVA) on unweighted
331 UniFrac distances was used to determine if samples grouped by *phase of experiment* were
332 significantly different from one another (*q2-beta-group-signifcance*). *Songbird*
333 (https://github.com/mortonjt/songbird) was employed to determine the importance (*i.e.,* fold
334 change) of each sOTU in relation to a given metadata variable (e.g., VREfm-colonisation).
335 Microbial features from all samples were split into training and test sets for supervised learning
336 classifier analyses; 20% of input samples were allocated to train the Random Forest Classifier
337 within QIIME2, the estimator method used for sample prediction. The different experimental
338 phases were the response variables, while the 16S rRNA gene data (and metabolomic spectra)
339 were the features.
340
341 *Metabolite extraction and liquid chromatography tandem mass-spectrometry analysis*
342 Duplicate fecal samples, as outlined in Table 1, were processed for polar metabolite extraction
343 and analysis (days 0, 5, 6, 7, 8, 9, and 14). Feces were metabolically arrested by immediate
344 collection into dry ice, and stored at -80˚C until further processing. Metabolite extraction from
345 the fecal samples was undertaken by the addition of 500 µL per sample of methanol:water
346 solution (3:1 v/v) containing 2µM ^{13}C-sorbitol and 8µM ^{13}C,^{15}N-valine, and 2µM ^{13}C-leucine
347 as internal standards. Fecal samples were homogenized at 1200 rpm for 30 minutes in a
348 thermomixer maintained at 4°C, and mechanically disrupted and incubated for a further 15
349 minutes in the thermomixer. Samples were randomized for metabolite extraction.

350 Metabolite analysis of the extracted samples and 13 mixtures of authentic standards
351 mixes was performed by liquid chromatography mass spectrometry (LC-MS), using
352 hydrophilic interaction column (ZIC-pHILIC) and high-resolution Agilent 6545 series
353 quadrupole time-of-flight mass spectrometry (QTOF MS) as described previously (25). Ions
354 were analyzed in positive mode with full scan range of 85 to 1200 m/z and in data-dependent
355 tandem MS mode to facilitate downstream metabolite identification. Mass spectrometry data
356 were deposited into *QIITA* (21) under the project title *Mouse-hospital VRE colonization with*
357 *ceftriaxone treatment* (Study ID 11737).
358
359 *Metabolomic analyses*
360 The data-dependent tandem MS data was processed using *MZmine2* (26) to generate tabular
361 matrices of metabolite features. Metabolomic features were further analysed within the *Global*
362 *Natural Products Social Networking (GNPS;* (13)*)* framework (UCSD, CA, USA). Tandem
363 MS data were processed for identification, dereplication and quantification, including spectral
364 library searches. For example, MS2 spectra of the unknown metabolites are compared with a
365 library of MSMS spectra generated from structurally characterized metabolites. Further
366 information on the GNPS workflow, and molecular networking can be found in Ming *et al.,*
367 2016 (13).
368
369 *Neural networking to predict microbe-metabolite interactions*
370 Microbiota and metabolome feature tables were analyzed using *MMVEC*
371 ((27)https://github.com/biocore/mmvec) to identify microbe-metabolite interactions through
372 their co-occurrence probabilities as predicted by neural networking. Conditional biplots were
373 generated using *Emperor*. Further, microbe abundances and metabolite log centered abundance

374 heatmaps were generated using primary derived data from multinomial regression analyses
375 using *Songbird* (https://github.com/mortonjt/songbird).
376

377 **Acknowledgements**
378 We thank the team at Metabolomics Australia (Bio21) mass spectrometry services. We thank
379 Dr. Daniel Petras (UCSD) for helpful discussions.
380

381 **Funding**
382 The project was supported by an Endeavour Research Fellowship (Australia Awards) for
383 collaborative research in the Department of Pediatrics at UCSD, CA, USA (ERF PDR
384 6735_2018) (AM). The project was also supported by the National Medical Research Council
385 of Australia, GNT1105525 (TPS) and GNT 1026656 (BPH). The funders had no role in study
386 design, data collection and interpretation, or the decision to submit the work for publication.
387

388 **References**
389

390 1. Arias CA, Murray BE. 2012. The rise of the Enterococcus: beyond vancomycin resistance.
391 Nat Rev Microbiol 10:266–278.
392

393 2. Panel G. 2017. Global priority list of antibiotic-resistant bacteria to guide research,
394 discovery, and development of new antibiotics. World Health Organization.
395

396 3. Ubeda C, Taur Y, Jenq RR, Equinda MJ, Son T, Samstein M, Viale A, Socci ND, van den
397 Brink M, Kamboj M, Pamer EG. 2010. Vancomycin-resistant Enterococcus domination of
398 intestinal microbiota is enabled by antibiotic treatment in mice and precedes bloodstream

399 invasion in humans. J Clin Invest 120:4332–4341.

400

401 4. Caballero S, Kim S, Carter RA, Leiner IM, Sušac B, Miller L, Kim GJ, Ling L, Pamer EG.
402 2017. Cooperating Commensals Restore Colonization Resistance to Vancomycin-Resistant
403 Enterococcus faecium. Cell Host Microbe 21:592-602.e4.

404

405 5. Ubeda C, Bucci V, Caballero S, Djukovic A, Toussaint NC, Equinda M, Lipuma L, Ling
406 L, Gobourne A, No D, Taur Y, Jenq RR, van den Brink MR, Xavier JB, Pamer EG. 2013.
407 Intestinal Microbiota Containing Barnesiella Species Cures Vancomycin-Resistant
408 Enterococcus faecium Colonization. Infect Immun 81:965–973.

409

410 6. Kim SG, Becattini S, Moody TU, Shliaha PV, Littmann ER, Seok R, Gjonbalaj M, Eaton
411 V, Fontana E, Amoretti L, Wright R, Caballero S, Wang Z-MX, Jung H-J, Morjaria SM,
412 Leiner IM, Qin W, Ramos RJ, Cross JR, Narushima S, Honda K, Peled JU, Hendrickson RC,
413 Taur Y, van den Brink MR, Pamer EG. 2019. Microbiota-derived lantibiotic restores
414 resistance against vancomycin-resistant Enterococcus. Nature 572:665–669.

415

416 7. Taur Y, Xavier JB, Lipuma L, Ubeda C, Goldberg J, Gobourne A, Lee Y, Dubin KA,
417 Socci ND, Viale A, Perales M-A, Jenq RR, van den Brink MR, Pamer EG. 2012. Intestinal
418 Domination and the Risk of Bacteremia in Patients Undergoing Allogeneic Hematopoietic
419 Stem Cell Transplantation. Clin Infect Dis 55:905–914.

420

421 8. Hildebrand F, Moitinho-Silva L, Blasche S, Jahn MT, Gossmann T, Huerta-Cepas J,
422 Hercog R, Luetge M, Bahram M, Pryszlak A, Alves RJ, Waszak SM, Zhu A, Ye L, Costea P,
423 Aalvink S, Belzer C, Forslund SK, Sunagawa S, Hentschel U, Merten C, Patil K, Benes V,

424 Bork P. 2019. Antibiotics-induced monodominance of a novel gut bacterial order. Gut
425 68:1781.
426
427 9. Brandl K, Plitas G, Mihu CN, Ubeda C, Jia T, Fleisher M, Schnabl B, DeMatteo RP,
428 Pamer EG. 2008. Vancomycin-resistant enterococci exploit antibiotic-induced innate immune
429 deficits. Nature 455:804–807.
430
431 10. Mundt OJ. 1963. Occurrence of Enterococci in animals in a wild environment. Appl
432 Microbiol 11.
433
434 11. Stinear TP, Olden DC, Johnson PD, Davies JK, Grayson LM. 2001. Enterococcal vanB
435 resistance locus in anaerobic bacteria in human faeces. Lancet 357:855–856.
436
437 12. Lozupone C, Knight R. 2005. UniFrac: a New Phylogenetic Method for Comparing
438 Microbial Communities. Appl Environ Microb 71:8228–8235.
439
440 13. Wang M, Carver JJ, Phelan VV, nchez L, Garg N, Peng Y, Nguyen D, Watrous J,
441 Kapono CA, Luzzatto-Knaan T, Porto C, Bouslimani A, Melnik AV, Meehan MJ, Liu W-T,
442 Crüsemann M, Boudreau PD, Esquenazi E, Sandoval-Calderón M, Kersten RD, Pace LA,
443 Quinn RA, Duncan KR, Hsu C-C, Floros DJ, Gavilan RG, Kleigrewe K, Northen T, Dutton
444 RJ, Parrot D, Carlson EE, Aigle B, Michelsen CF, Jelsbak L, Sohlenkamp C, Pevzner P,
445 Edlund A, McLean J, Piel J, Murphy BT, Gerwick L, Liaw C-C, Yang Y-L, Humpf H-U,
446 Maansson M, Keyzers RA, Sims AC, Johnson AR, debottom A, Sedio BE, Klitgaard A,
447 Larson CB, Cristopher BA, Torres-Mendoza D, Gonzalez DJ, Silva DB, Marques LM,
448 Demarque DP, Pociute E, O'Neill EC, Briand E, Helfrich EJ, Granatosky EA, Glukhov E,

449 Ryffel F, Houson H, Mohimani H, Kharbush JJ, Zeng Y, Vorholt JA, Kurita KL, Charusanti
450 P, McPhail KL, Nielsen K, Vuong L, Elfeki M, Traxler MF, Engene N, Koyama N, Vining
451 OB, Baric R, Silva RR, Mascuch SJ, Tomasi S, Jenkins S, Macherla V, Hoffman T, Agarwal
452 V, Williams PG, Dai J, Neupane R, Gurr J, Rodríguez AM, Lamsa A, Zhang C, Dorrestein K,
453 ggan B, Almaliti J, Allard P-M, Phapale P, Nothias L-F, Alexandrov T, Litaudon M,
454 Wolfender J-L, Kyle JE, Metz TO, Peryea T, Nguyen D-T, VanLeer D, Shinn P, Jadhav A,
455 Müller R, Waters KM, Shi W, Liu X, Zhang L, Knight R, Jensen PR, Palsson B, Pogliano K,
456 Linington RG, Gutiérrez M, Lopes NP, Gerwick WH, Moore BS, Dorrestein PC, Bandeira N.
457 2016. Sharing and community curation of mass spectrometry data with Global Natural
458 Products Social Molecular Networking. Nat Biotechnol 34:828–837.
459
460 14. Karki S, Houston L, Land G, Bass P, Kehoe R, Borrell S, Watson K, Spelman D, Kennon
461 J, Harrington G, Cheng AC. 2012. Prevalence and risk factors for VRE colonisation in a
462 tertiary hospital in Melbourne, Australia: a cross sectional study. Antimicrob Resist In 1:31.
463
464 15. Dubin K, Pamer EG. 2017. Enterococci and Their Interactions with the Intestinal
465 Microbiome. Microbiol Spectr 5.
466
467 16. Morton JT, Marotz C, Washburne A, Silverman J, Zaramela LS, Edlund A, Zengler K,
468 Knight R. 2019. Establishing microbial composition measurement standards with reference
469 frames. Nat Commun 10:2719.
470
471 17. Amir A, nald D, Navas-Molina JA, Kopylova E, Morton JT, Xu Z, Kightley EP,
472 Thompson LR, Hyde ER, Gonzalez A, Knight R. 2017. Deblur Rapidly Resolves Single-
473 Nucleotide Community Sequence Patterns. Msystems 2:e00191-16.

18. Morrison DJ, Preston T. 2016. Formation of short chain fatty acids by the gut microbiota and their impact on human metabolism. Gut Microbes 7:189–200.

19. Dubin KA, Mathur D, McKenney PT, Taylor BP, Littmann ER, Peled JU, van den Brink MR, Taur Y, Pamer EG, Xavier JB. 2019. Diversification and Evolution of Vancomycin-Resistant Enterococcus faecium during Intestinal Domination. Infect Immun 87.

20. Thompson LR, Sanders JG, nald D, Amir A, Ladau J, Locey KJ, Prill RJ, Tripathi A, Gibbons SM, Ackermann G, Navas-Molina JA, Janssen S, Kopylova E, Vázquez-Baeza Y, González A, Morton JT, Mirarab S, Xu Z, Jiang L, Haroon MF, Kanbar J, Zhu Q, Song S, Kosciolek T, Bokulich NA, Lefler J, Brislawn CJ, Humphrey G, Owens SM, Hampton-Marcell J, Berg-Lyons D, McKenzie V, Fierer N, Fuhrman JA, Clauset A, Stevens RL, Shade A, Pollard KS, Goodwin KD, Jansson JK, Gilbert JA, Knight R, Rivera JL, Al-Moosawi L, Alverdy J, Amato KR, Andras J, Angenent LT, Antonopoulos DA, Apprill A, Armitage D, Ballantine K, Bárta J, Baum JK, Berry A, Bhatnagar A, Bhatnagar M, Biddle JF, Bittner L, Boldgiv B, Bottos E, Boyer DM, Braun J, Brazelton W, Brearley FQ, Campbell AH, Caporaso GJ, Cardona C, Carroll J, Cary CS, Casper BB, Charles TC, Chu H, Claar DC, Clark RG, Clayton JB, Clemente JC, Cochran A, Coleman ML, Collins G, Colwell RR, Contreras M, Crary BB, Creer S, Cristol DA, Crump BC, Cui D, Daly SE, Davalos L, Dawson RD, Defazio J, Delsuc F, Dionisi HM, Dominguez-Bello M, Dowell R, Dubinsky EA, Dunn PO, Ercolini D, Espinoza RE, Ezenwa V, Fenner N, Findlay HS, Fleming ID, Fogliano V, Forsman A, Freeman C, Friedman ES, Galindo G, Garcia L, Garcia-Amado M, Garshelis D, Gasser RB, Gerdts G, Gibson MK, Gifford I, Gill RT, Giray T, Gittel A, Golyshin P, Gong D, Grossart H-P, Guyton K, Haig S-J, Hale V, Hall R, Hallam SJ, Handley

499 KM, Hasan NA, Haydon SR, Hickman JE, Hidalgo G, Hofmockel KS, Hooker J, Hulth S,
500 Hultman J, Hyde E, Ibáñez-Álamo J, Jastrow JD, Jex AR, Johnson SL, Johnston ER, Joseph
501 S, Jurburg SD, Jurelevicius D, Karlsson A, Karlsson R, Kauppinen S, Kellogg CT, Kennedy
502 SJ, Kerkhof LJ, King GM, Kling GW, Koehler AV, Krezalek M, Kueneman J, Lamendella
503 R, Landon EM, Lane-deGraaf K, LaRoche J, Larsen P, Laverock B, Lax S, Lentino M, Levin
504 II, Liancourt P, Liang W, Linz AM, Lipson DA, Liu Y, Lladser ME, Lozada M, Spirito CM,
505 MacCormack WP, MacRae-Crerar A, Magris M, Martín-Platero AM, Martín-Vivaldi M,
506 Martínez ML, Martínez-Bueno M, Marzinelli EM, Mason OU, Mayer GD, vitt-Irwin JM,
507 nald JE, McGuire KL, McMahon KD, McMinds R, Medina M, Mendelson JR, Metcalf JL,
508 Meyer F, Michelangeli F, Miller K, Mills DA, Minich J, Mocali S, Moitinho-Silva L, Moore
509 A, Morgan-Kiss RM, Munroe P, Myrold D, Neufeld JD, Ni Y, Nicol GW, Nielsen S,
510 Nissimov JI, Niu K, Nolan MJ, Noyce K, O'Brien SL, Okamoto N, Orlando L, Castellano Y,
511 Osuolale O, Oswald W, Parnell J, Peralta-Sánchez JM, Petraitis P, Pfister C, Pilon-Smits E,
512 Piombino P, Pointing SB, Pollock JF, Potter C, Prithiviraj B, Quince C, Rani A, Ranjan R,
513 Rao S, Rees AP, Richardson M, Riebesell U, Robinson C, Rockne KJ, Rodriguezl S, Rohwer
514 F, Roundstone W, Safran RJ, Sangwan N, Sanz V, Schrenk M, Schrenzel MD, Scott NM,
515 Seger RL, Seguin-Orlando A, Seldin L, Seyler LM, Shakhsheer B, Sheets GM, Shen C, Shi
516 Y, Shin H, Shogan BD, Shutler D, Siegel J, Simmons S, Sjöling S, Smith DP, Soler JJ,
517 Sperling M, Steinberg PD, Stephens B, Stevens MA, Taghavi S, Tai V, Tait K, Tan CL, Tas¸
518 N, Taylor LD, Thomas T, Timling I, Turner BL, Urich T, Ursell LK, van der Lelie D,
519 Treuren W, van Zwieten L, Vargas-Robles D, Thurber R, Vitaglione P, Walker DA, Walters
520 WA, Wang S, Wang T, Weaver T, Webster NS, Wehrle B, Weisenhorn P, Weiss S, Werner
521 JJ, West K, Whitehead A, Whitehead SR, Whittingham LA, Willerslev E, Williams AE,
522 Wood SA, Woodhams DC, Yang Y, Zaneveld J, Zarraonaindia I, Zhang Q, Zhao H. 2017. A
523 communal catalogue reveals Earth's multiscale microbial diversity. Nature 551:457–463.

21. Gonzalez A, Navas-Molina JA, Kosciolek T, nald D, Vázquez-Baeza Y, Ackermann G, DeReus J, Janssen S, Swafford AD, Orchanian SB, Sanders JG, Shorenstein J, Holste H, Petrus S, Robbins-Pianka A, Brislawn CJ, Wang M, Rideout J, Bolyen E, Dillon M, Caporaso GJ, Dorrestein PC, Knight R. 2018. Qiita: rapid, web-enabled microbiome meta-analysis. Nat Methods 15:796–798.

22. Bolyen E, Rideout J, Dillon MR, Bokulich NA, Abnet CC, Al-Ghalith GA, Alexander H, Alm EJ, Arumugam M, Asnicar F, Bai Y, Bisanz JE, Bittinger K, Brejnrod A, Brislawn CJ, Brown TC, Callahan BJ, Caraballo-Rodríguez A, Chase J, Cope EK, Silva R, Diener C, Dorrestein PC, Douglas GM, Durall DM, Duvallet C, Edwardson CF, Ernst M, Estaki M, Fouquier J, Gauglitz JM, Gibbons SM, Gibson DL, Gonzalez A, Gorlick K, Guo J, Hillmann B, Holmes S, Holste H, Huttenhower C, Huttley GA, Janssen S, Jarmusch AK, Jiang L, Kaehler BD, Kang K, Keefe CR, Keim P, Kelley ST, Knights D, Koester I, Kosciolek T, Kreps J, Langille MG, Lee J, Ley R, Liu Y-X, Loftfield E, Lozupone C, Maher M, Marotz C, Martin BD, nald D, McIver LJ, Melnik AV, Metcalf JL, Morgan SC, Morton JT, Naimey A, Navas-Molina JA, Nothias L, Orchanian SB, Pearson T, Peoples SL, Petras D, Preuss M, Pruesse E, Rasmussen L, Rivers A, Robeson MS, Rosenthal P, Segata N, Shaffer M, Shiffer A, Sinha R, Song S, Spear JR, Swafford AD, Thompson LR, Torres PJ, Trinh P, Tripathi A, Turnbaugh PJ, Ul-Hasan S, van der Hooft JJ, Vargas F, Vázquez-Baeza Y, Vogtmann E, von Hippel M, Walters W, Wan Y, Wang M, Warren J, Weber KC, Williamson CH, Willis AD, Xu Z, Zaneveld JR, Zhang Y, Zhu Q, Knight R, Caporaso GJ. 2019. Reproducible, interactive, scalable and extensible microbiome data science using QIIME 2. Nat Biotechnol 37:852–857.

549 23. Pedregosa F, Varoquaux G, Gramfort A, Michel V, Thirion B, Grisel O, Blondel M,
550 Müller A, Nothman J, Louppe G, Prettenhofer P, Weiss R, Dubourg V, Vanderplas J, Passos
551 A, Cournapeau D, Brucher M, Perrot M, Duchesnay É. 2012. Scikit-learn: Machine Learning
552 in Python.
553
554 24. Janssen S, nald D, Gonzalez A, Navas-Molina JA, Jiang L, Xu Z, Winker K, Kado DM,
555 Orwoll E, Manary M, Mirarab S, Knight R. 2018. Phylogenetic Placement of Exact
556 Amplicon Sequences Improves Associations with Clinical Information. Msystems 3:e00021-
557 18.
558
559 25. Masukagami Y, Nijagal B, Mahdizadeh S, Tseng C-W, Dayalan S, Tivendale KA,
560 Markham PF, Browning GF, Sansom FM. 2019. A combined metabolomic and bioinformatic
561 approach to investigate the function of transport proteins of the important pathogen
562 Mycoplasma bovis. Vet Microbiol 234:8–16.
563
564 26. Pluskal T, Castillo S, Villar-Briones A, Orešič M. 2010. MZmine 2: Modular framework
565 for processing, visualizing, and analyzing mass spectrometry-based molecular profile data.
566 Bmc Bioinformatics 11:395.
567
568 27. Morton JT, Aksenov AA, Nothias L, Foulds JR, Quinn RA, Badri MH, Swenson TL,
569 Goethem MW, Northen TR, Vazquez-Baeza Y, Wang M, Bokulich NA, Watters A, Song S,
570 Bonneau R, Dorrestein PC, Knight R. 2019. Learning representations of microbe–metabolite
571 interactions. Nat Methods 1–9.
572
573

574

575

Day of experiment	0	1	2	3	4	5	6	7	8	9	10	11	12	13	14
Phase of experiment*	N	N	N	N	N	N	Abx-Tx	Abx-Tx	Abx-Wn	VRE-E	VRE-E	VRE-E	VRE-E	VRE-L	VRE-L
Amplicon 16S rRNA gene data	✓	✓	✓	-	-	✓	✓	✓	✓	✓	-	-	✓	✓	✓
Metabolomics	✓	-	-	-	-	✓	✓	✓	✓	✓	-	-	-	-	✓
Avg observed sOTUs#	210	220	220	-	-	225	112	84	93	30	-	-	22	34	53

576

577 **Table 1:** Summary of samples analyzed in this study

578 Notes: *The key phases of the experiment where, N represents Naïve; Abx-Tx represents Antibiotic treatment; Abx-Wn represents Antibiotic weaning;

579 VRE-E represents Early-phase post-VREfm colonisation; and VRE-L represents Late-phase post-VREfm colonization; #The average number of sOTUs

580 observed across all mice for each day of the experiment; '✓' Sample processed; '-' Data unavailable

581 **Figures**

582

583 **Fig. 1**

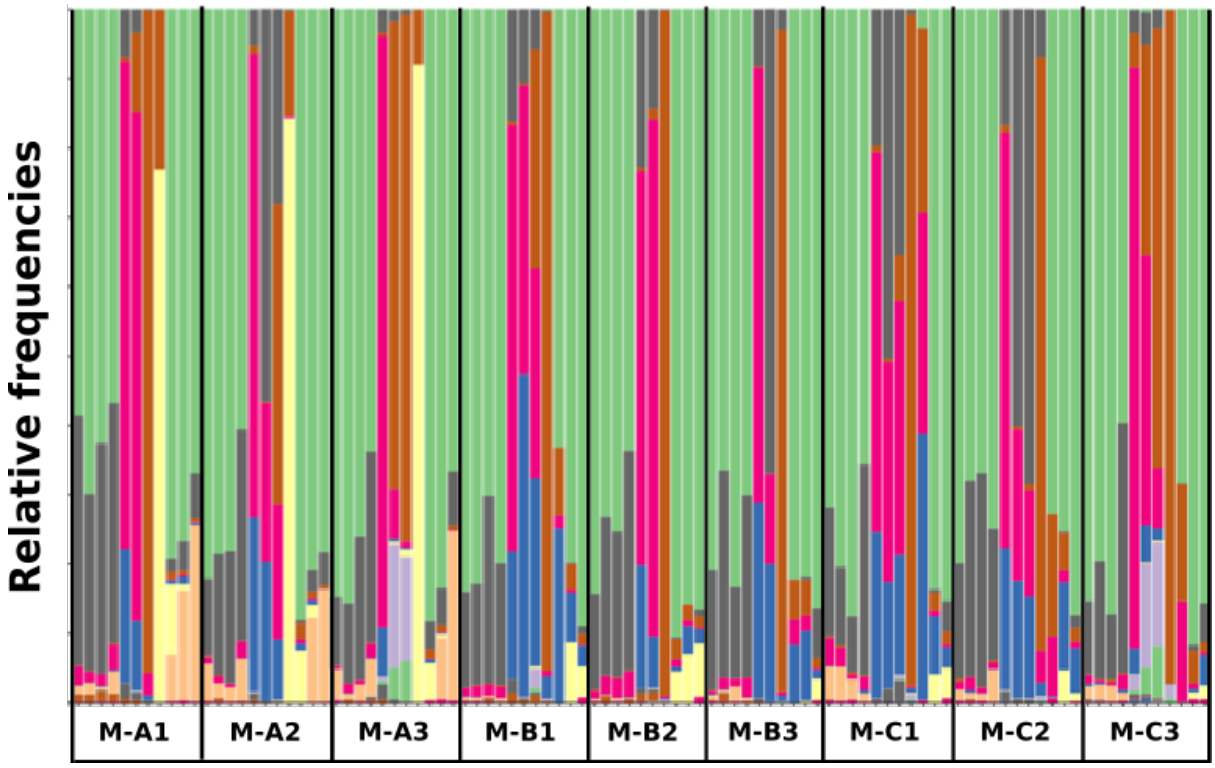

584

585

586 **Figure 1 Biodiversity plot of sOTUs as relative frequencies at the taxonomic level of Class.**
587 First-order shifts in microbial community composition, as revealed by 16S rRNA community
588 profiling, from a predominance of Bacteroidetes to Tenericutes and return to Bacteroidetes was
589 observed. Each column displays the relative bacterial community composition in a mouse
590 faecal sample collected at daily intervals, and sorted by the chronology of the experiment (i.e.,
591 Day of experiment; Table 1). 'M-A1' notation refers to the box and mouse number; for
592 example, M-A1 is mouse 1 in Group A, while M-B2 is mouse 2 in Group B. The colors
593 represent different bacterial classes, including Bacteroidia (green), Clostridia (grey)
594 Tenericutes (Mollicutes; pink), Bacilli (brown), and gamma-Proteobacteria (yellow).

595

596 **Fig. 2**

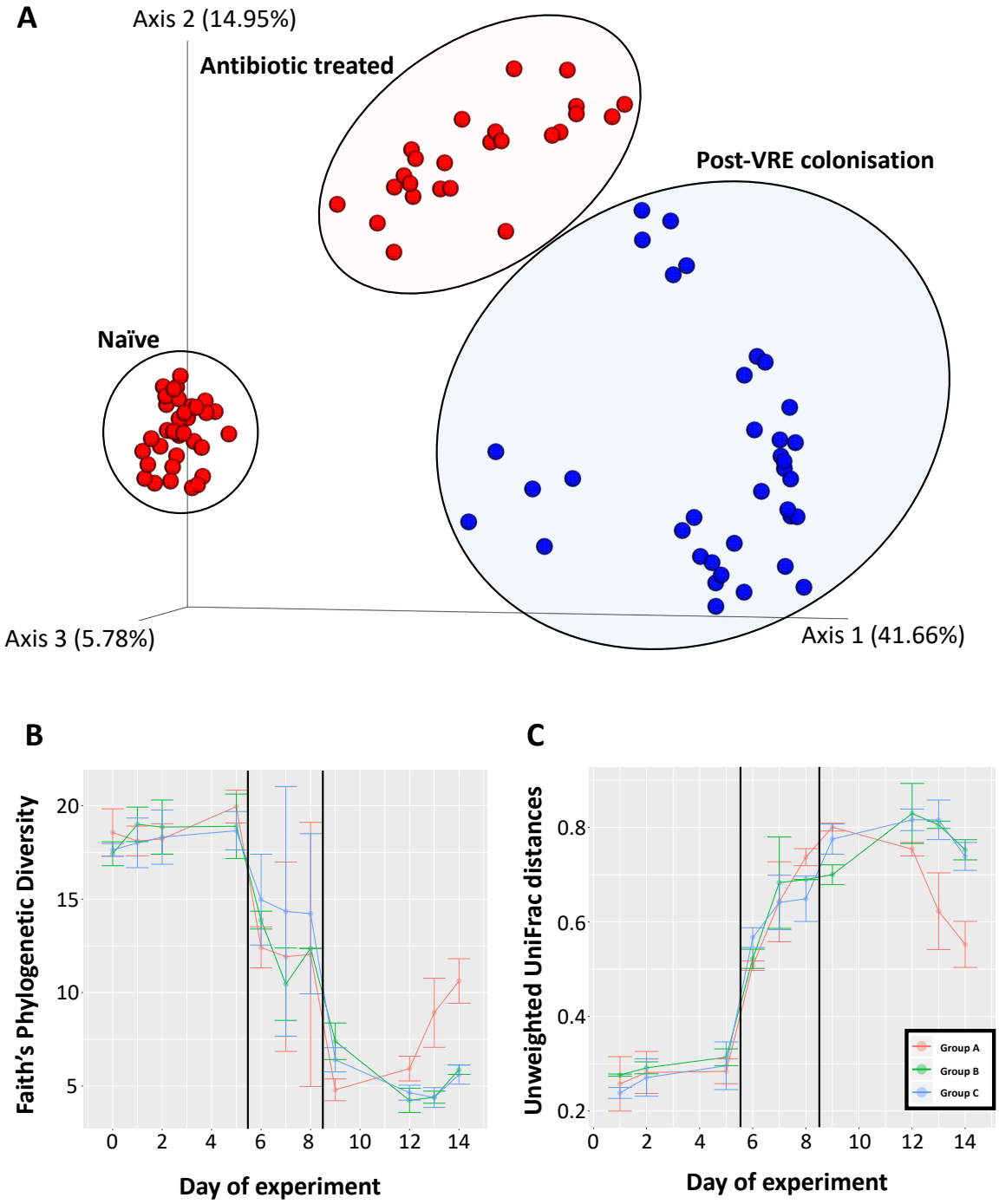

597 **Figure 2 Diversity analyses.** (A) Principal coordinate analysis plot of unweighted UniFrac
598 distances. Data points are projected onto the sample space, and coloured by pre-VREfm
599 colonisation (red), and post-VREfm colonisation (blue). *n.b.,* circles and ellipses function to
600 highlight the separation of experimental phases and do not indicate statistical confidence
601 intervals. Principal coordinate axis 1 explains 41.66% of the variation observed between the

602 naïve microbiota and those from the post-VREfm colonisation phase. (B) Community richness
603 of the murine gut microbiome, as measured by Faith's Phylogenetic Diversity, in response to
604 ceftriaxone treatment and challenge with VREfm; (C) community dissimilarity distances, as
605 calculated by unweighted UniFrac, of each time point relative to day 0 (naïve phase).
606

607 **Fig. 3**

Positively associated with colonisation	
Enterococcus	1.6693
Bacteroides	1.0559
Erysipelotrichaceae	1.0521
Catabacter	0.8159
Lachnospiraceae	0.7848
Negative association with colonisation	
Clostridiales	-4.0947
Adlercreutzia	-3.8292
Mollicutes	-3.8392
Peptostreptococcaceae	-3.7357
Clostridiales	-3.5084

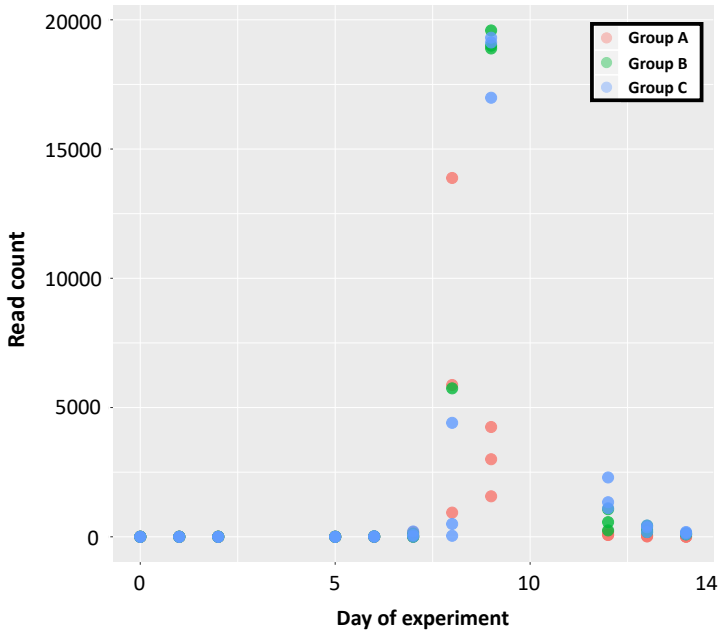

608

609 **Figure 3 Multinomial regression.** Multinomial regression identified an *Enterococci* exact
610 sequence variant as the most positively associated with the colonisation phase (log-fold change
611 score of 1.6693). Read counts for the *Enterococci*-ESV tracked daily across the experiment
612 showing high abundance during days of VREfm challenge.

613

614

615 **Fig. 4**

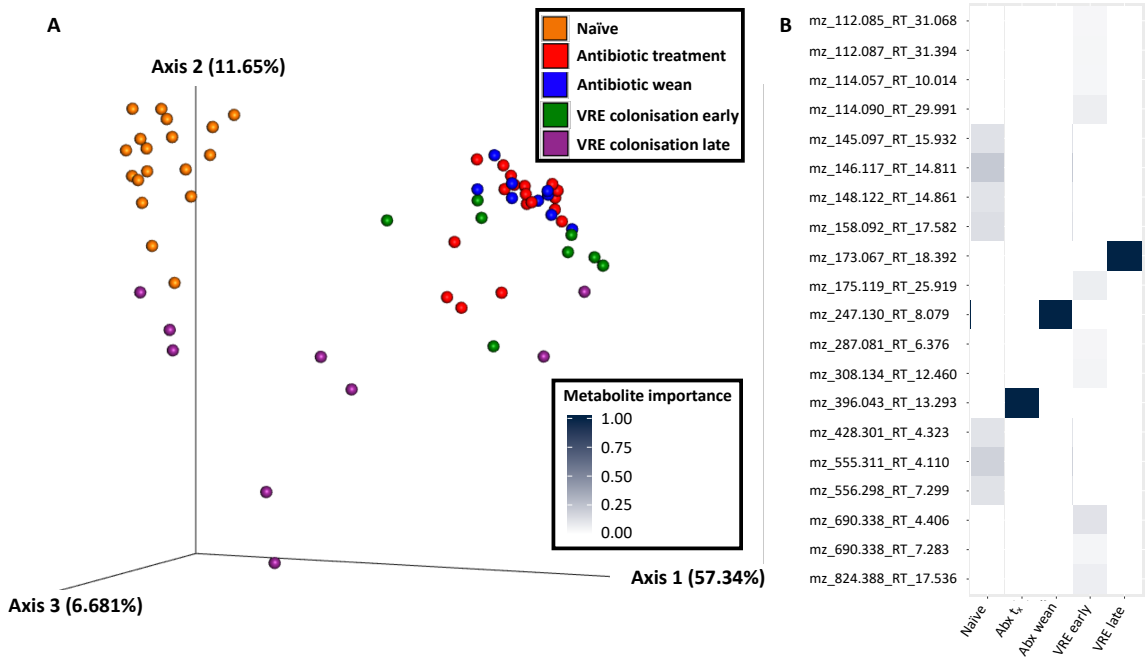

616

617 **Figure 4 Metabolomic analyses.** (A) Emperor plot displaying principal coordinate analysis of
618 binary Jaccard distances of metabolomic profiles. Samples represent (colour coded) the naïve
619 (orange), antibiotic-treatment (red), antibiotic-weaning (blue), early-VRE colonisation (green),
620 and late-VREfm colonisation (purple) phases. (B) Random Forest classifier identifying
621 metabolite features (spectra) for each phase of the experiment. Heatmap is colour-coded from
622 low ranking score (white; i.e., lowest importance) to high ranking score (dark blue; highest
623 importance). Metabolite features are labelled by their mass-charge ratios and retention times
624 for the reason that current databases do not capture their chemical structure and/or
625 identifications.

626

627

628 **Fig. 5**

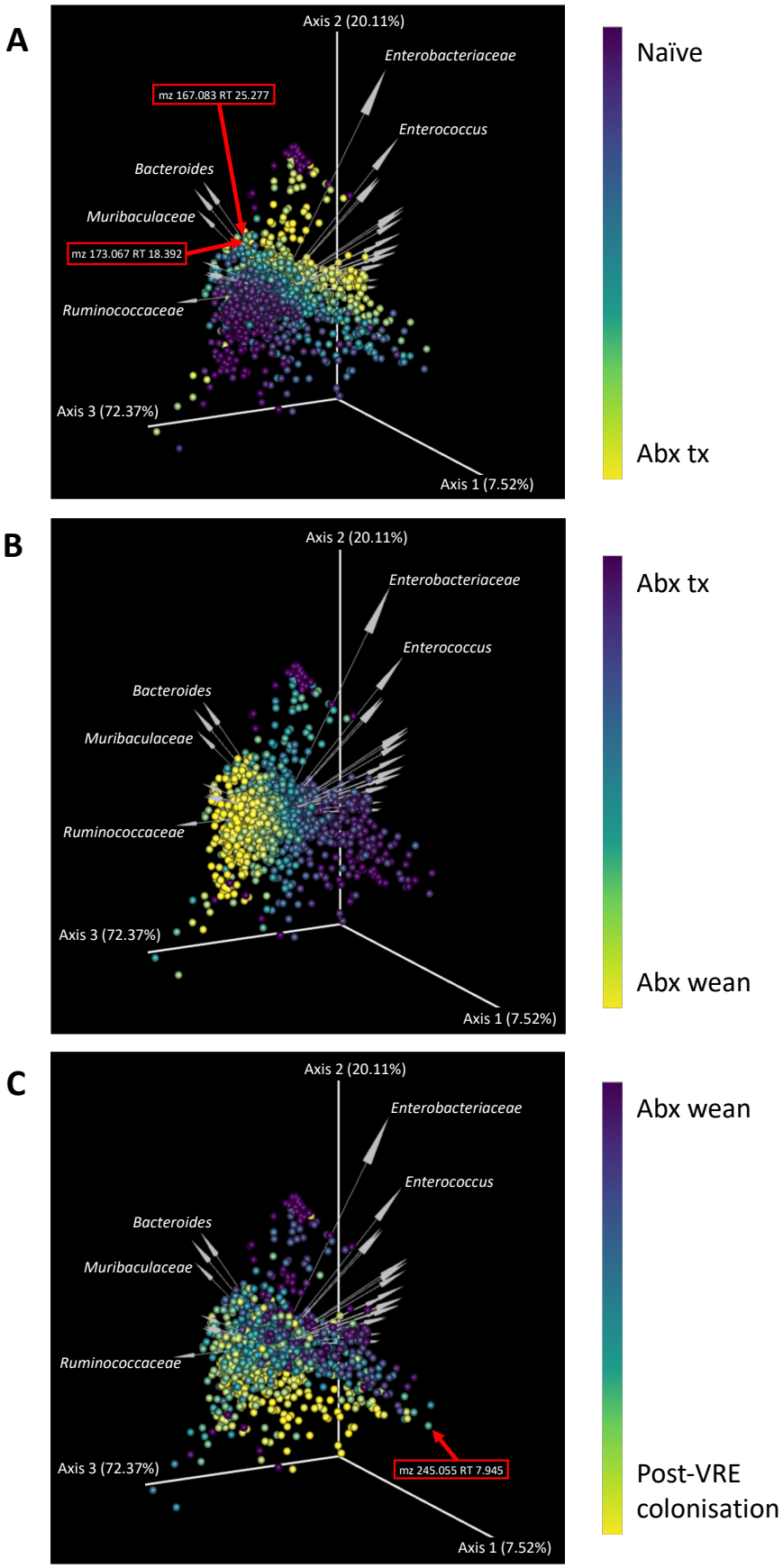
A
Axis 2 (20.11%)
Enterobacteriaceae
mz 167.083 RT 25.277
Enterococcus
Bacteroides
Muribaculaceae
mz 173.067 RT 18.392
Ruminococcaceae
Axis 3 (72.37%)
Axis 1 (7.52%)
Naïve
Abx tx
B
Axis 2 (20.11%)
Enterobacteriaceae
Enterococcus
Bacteroides
Muribaculaceae
Ruminococcaceae
Axis 3 (72.37%)
Axis 1 (7.52%)
Abx tx
Abx wean
C
Axis 2 (20.11%)
Enterobacteriaceae
Enterococcus
Bacteroides
Muribaculaceae
Ruminococcaceae
Axis 3 (72.37%)
mz 245.055 RT 7.945
Axis 1 (7.52%)
Abx wean
Post-VRE colonisation

629 **Figure 5 Microbe-metabolite vector biplots.** Sequential biplots highlighting the changing
630 metabolite differentials across each key phase of the experiment; where *abx tx* corresponds to
631 the *antibiotic treatment* phase, and *abx wean* corresponds to the period where antibiotics were
632 removed for a 24-hour period prior to colonisation with VREfm. Each point on the sample
633 space represents metabolites, and arrows represent microbes. Microbe and metabolite features
634 are fixed upon the sample space, with gradient coloring of metabolites indicating the transition
635 across key phases of the experiment. The distance between each point is indicative of
636 metabolite co-occurrence frequency, and the angle between arrows indicate microbial co-
637 occurrence. The directionality of the arrows describes the variation in the metabolites explained
638 the microbes represented by the arrows. For example, metabolite mz 173.067 RT 18.392 is
639 demonstrated to co-occur with *Bacteroides*.
640
641

642 **Supplementary figures**

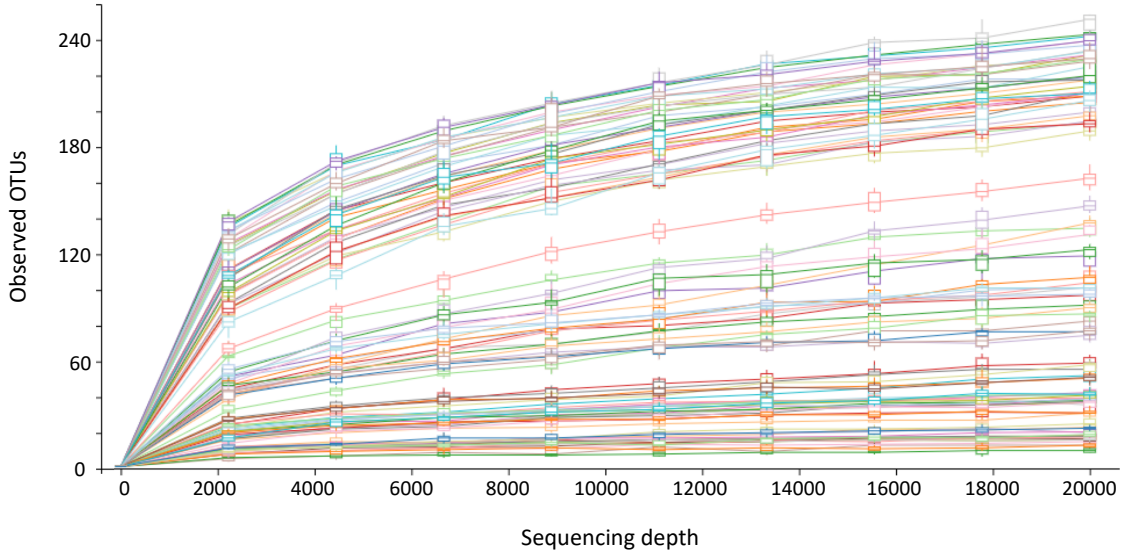

643

644 **Supplementary Figure 1** Alpha rarefaction plot of all samples rarefied to 20,000 reads per

645 sample.

646

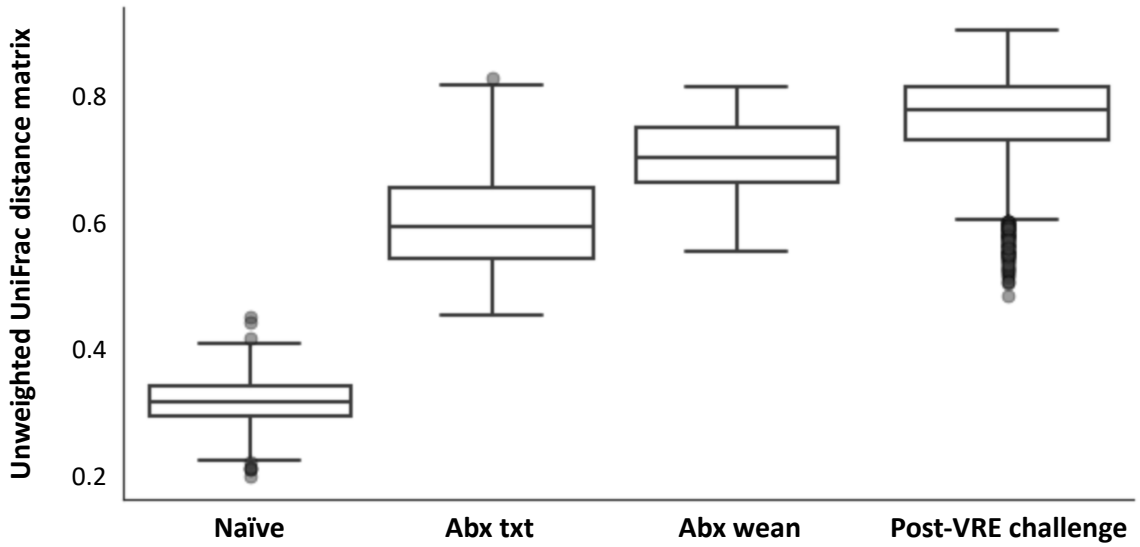

647 **Supplementary Figure 2** PERMANOVA testing (999 permutations) on unweighted UniFrac

648 distances relative to samples from the naïve phase. P-values for pairwise PERMANOVA

649 testing given in parentheses for the following phases of the experiment: naïve – antibiotic

650 treatment (0.001); naïve – antibiotic treatment (0.001); naïve – infection (0.001); antibiotic

651 treatment – antibiotic wean (0.025).

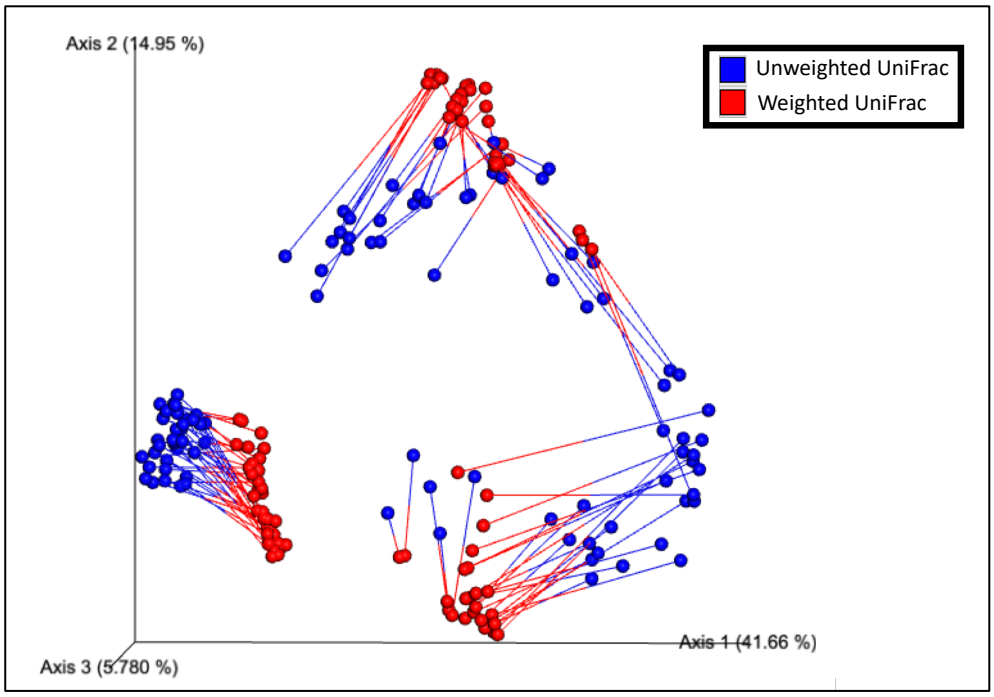

Supplementary Figure 3 Emperor plot of procrustes analysis of unweighted (blue) and weighted (red) UniFrac distance metrices.

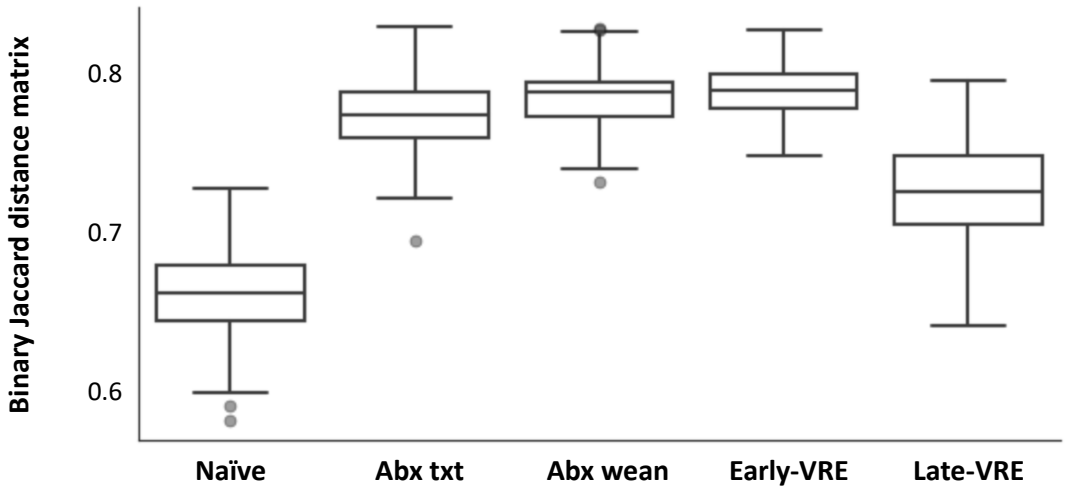

Supplementary Figure 4 Pairwise PERMANOVA testing (999 permutations) on binary Jaccard distances relative to samples from the naïve phase. While naïve and late-VRE samples are significantly different, late-VRE has a lower distance to naïve compared to Abx txt, Abx wean and early-VRE samples.

677

678

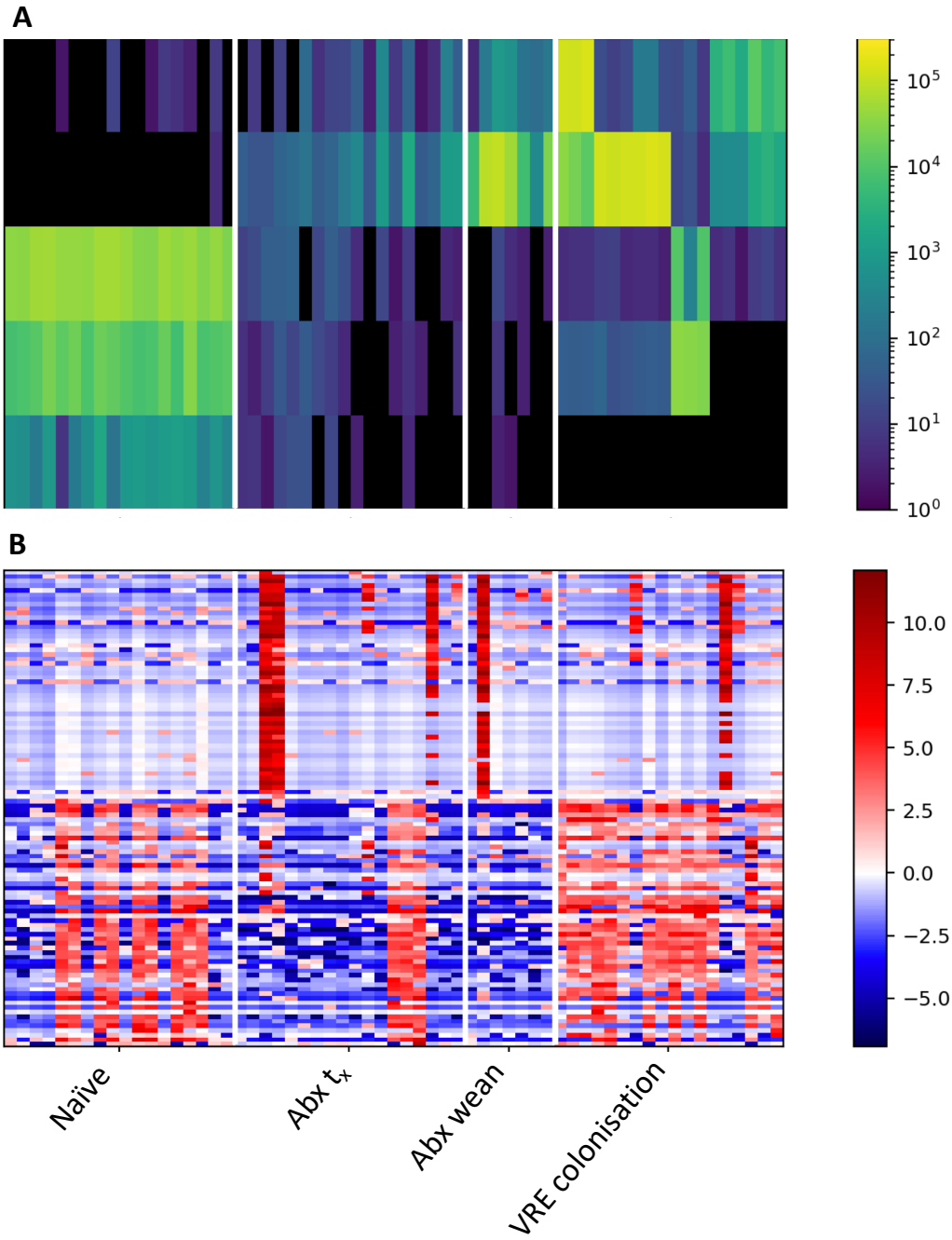

679

680 **Supplementary Figure 5 Feature abundances.** (A) Microbe abundances and (B) metabolite

681 log centered abundances across each phase of the experiment.

682

683